INVESTIGATING THE SUITABILITY OF A TWO DIMENSIONAL SMALL SIZE VERTICAL AXIS WIND TURBINE NUMERICAL MODEL

Okeoghene Eboibi

08069477913, o.eboibi@gmail.com
Department of Mechanical Engineering,
Delta State University of Science and Technology, Ozoro

ABSTRACT

This paper aims at the determination of the suitability of applying a numerical model of a VAWT for research purpose. A CFD two dimensional model was created and simulated with fluent code software while the forces and flow field data were monitored and obtained. The data were compared with the experimental data obtained from a wind tunnel test. Data comprised forces and flow field velocity of a similar sized VAWT were experimental obtained in a wind tunnel, through suitable VAWT performance measurements and particle image velocimetry techniques. The suitability procedure was initiated with a static aerofoil study that reduced five fully turbulence models to one by the comparison of the fully turbulence models against experimental data at Reynolds number of $1.35x10^5$. The Transition SST and SST k-w models data sets of VAWT model were thereafter compared to the force and PIV experimental data of similar scaled VAWT obtained in a wind tunnel. The force and flow physics verification and validation show the Transition SST turbulence model as the most appropriate model for CFD modelling at the Reynolds numbers of $1.27x10^3$, thus confirming that numerical methods are valuable tools that can be used in conducting research in VAWT.

Keywords: Computational Fluid Dynamics, Vertical Axis Wind Turbine, Particle Image Velocimentry, Flow physics, Performance

Introduction

Wind is a natural resource that could be harnessed to generate clean energy. The harvest of energy from wind can positively affect the cleanliness of the environment by reducing the emissions from the burning of fossil fuels particularly in the underdeveloped and developing nations that have inadequate power to cater for the needs of their populations. The massive exploration and processing of fossil fuels could cause their scarcity in the near future. This has led to seeking an alternative means of producing diesel and other petroleum products; and are being researched into to cushion the effects of non-availability of the natural fossil fuel (Eboibi et al., 2018). Wind resources is free and unlike the fossil fuel that must be extracted and processed before use. For the application and installation of wind harvesting devices in the near future. The area needs to be evaluated to determine the suitability and profitability of wind harvest in such location (Eboibi et al., 2017). Wind is renewable resources and investment into the industry can significantly contribute to employment and indirectly increase the gross domestic product of a country

Wind turbine is a device that converts energy from the wind to electricity. There are two broad types, the horizontal axis wind turbines (HAWT) and the vertical axis wind turbines (VAWT). The HAWTs are common and established due to many years of research while there is a resurgence of research interest into the VAWT recently because of the numerous advantages the VAWT has over the HAWT (Qing' an et al., 2016, Eboibi O., 2016, Sungjun et. al 2015).
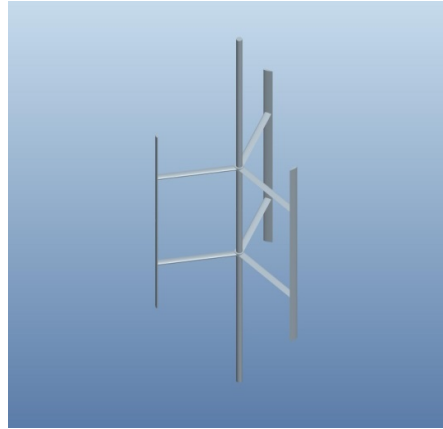
Figure 1: A typical three bladed vertical wind turbine card model

The Figure 1 shows a card model of three bladed VAWT with, it can receive wind from all the direction so does not need a yaw mechanism to propel it into the direction of wind. The blades are straight and uniform therefore easy to design and manufacture. Due to low rotational speed, the noise associated with the VAWT is low. The disadvantage of the VAWT is its inability to self-start and the complex aerodynamics that is caused by the rapid changes in the flow field and angular velocity.

Experimental methods is limited by huge capital cost requirements, an array of diverse technical skills, time constrains, operational know-how, and a number of physical and environmental parameters that can influence measurements. Despite these shortcomings associated with experimental methods, it is still acclaimed the most reliable method of investigation, which can be carried out by either field or laboratory tests (Eboibi, 2013).

Due to the limitation of conducting experiments, numerical methods have been applied in the investigation of VAWTs. Computation Fluid Dynamics (CFD) is a recent numerical method applied in the study of VAWT. The CFD software has equally been enhanced by advances in computational hardware so the benefits derived from CFD is all comprising. CFD is not limited to its application in evaluation, optimisation and performance determination to solve problems of existing VAWT, but it is also used to create and visualise a virtual prototype of a VAWT that can give insight into the design and performance which may not be possible with other investigative methods.

CFD has the flexibility by which the design can be altered to test various desired conditions for analytical purposes, and the facility of calculating aerodynamic lift and drag forces on blades so does not rely on external data set for further analysis, which is seen as a very major advantage when

compared with other numerical methods. Despite these advantages presented by CFD, its results of simulated models must be verified and validated with those of laboratory and experimental models at similar tests conditions to assess performance, aerodynamics and aptness of such designs for research and commercial purposes.

Raciti-Castelli et al, (2010), and Howell, (2010) made attempts at verifying various CFD models against measured data in wind tunnel. The validation was purely a comparison exercise where only one turbulence model was compared with measured wind tunnel forces and there was no comparison of the physics associated with the flow. So the privilege of an appropriate choice of turbulence model from the validation procedure is very limited due to the comparison of numerical and experimental data of only one turbulence model.

Howell et al. (2010) conducted their experiments in the low speed wind tunnel that houses a three bladed VAWT with NACA0022 profile. Surface roughens and solidity were tested at various λ and wind speeds that was deemed realistic. The data obtained from the experiment was verified with the simulation results of a 2D and 3D CFD models. Their results was insightful of the understanding of VAWT performance especially in relation to the tested parameters, but the selection process of the RNG $k - \varepsilon$ turbulence model was not scientific because the yardstick used for the selection of the turbulence model is generalised.

Raciti-Castelli (2010) carried out their experimental investigation in a low turbulence wind tunnel laboratory. A three bladed VAWT with NACA0021 profile was tested and forces was monitored over λ that ranges between 1.0 to 3.5 at 9m/s. The obtained experimental data and that of the two dimensional CFD model simulation that used enhanced wall treatment $k - \varepsilon$ Realisable turbulence model were compared. Again, the choice of the turbulence model was based on

available information from the CFD software documentation.

Sumgjun et. al (2015) validated their numerical model by comparison of the numerical results with the experimental data of Howell et al. (2010). The validation showed closeness of both the experimental and numerical torque. The authors (Sumgjun et. al., 2015) did not verify their model with flow field and an analysis for the choice of suitable turbulence model was not shown. Jian et.al., (2016) studied VAWT performance improvement through assessment of the aerofoil family, like the work of Sungjun et al. (2016), there was no flow field verification of the numerical model but in the authors discussed results plots flow field of different aerofoil were presented that enabled the conclusion of their study.

This paper seeks to investigate the suitability of a 2D VAWT CFD model for research by the validation and verification of the created model through the development of an applicable two dimensional VAWT CFD model by using and appropriate software, the developed CFD model shall be modelled with the commercial fluent code commercial software. The forces and flow features with different types of turbulence models will monitored in the simulation process. Thereafter experimental tests that measured the forces and flow filed were conducted on a similar sized laboratory VAWT model under the same test conditions. The CFD and the experimental data were compared to ascertain the applicable and suitable turbulence model to confirm the suitability of the numerical model for research.

Numerical methods

Model

The numerical investigation was designed around a two dimensional computational domain simulating flow through the turbine's cross section. The computational domain contained a rotating inner sub-domain embedded within 1.5m from the velocity inlet boundary and 3m from the pressure outlet boundary (Figure 2). The rotor has a diameter of 0.727m and incorporated a 0.027m diameter central shaft.

The set 3m distance is considered appropriate to ensure that the wake development is not terminated prematurely despite revelation that no appreciable changes in torque was observed when the outlet boundary is set at $do \geq 2$m from the VAWT axis. The walls of the side were defined as no-slip wall and set at 1.2m apart from the axis of rotation of the VAWT. The 1.2m distance of the side walls was adopted since it equals the blockage ratio when compared to the actual 3D wind tunnel setup and also in agreement with the sidewall investigation by Danao (2013) on a similar VAWT model of the same wind tunnel.
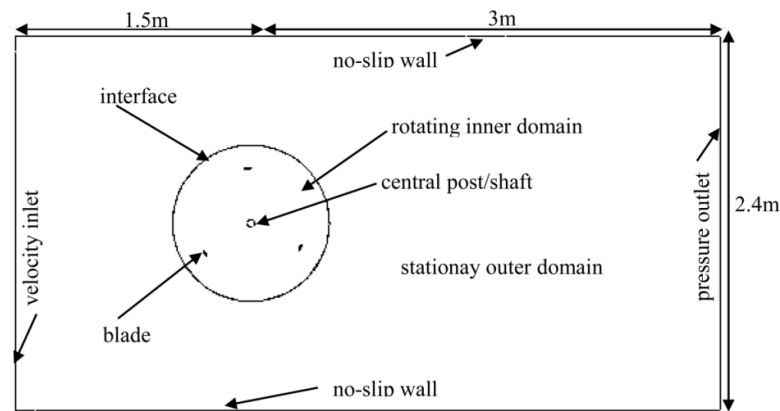
Figure 2: The 2D CFD model boundaries and the features

A sliding mesh interface is present on the boundary between the two sub-domains. The three aerofoils contained in the rotating inner domain is embedded in an O-type mesh of 60 layers (Figure 3) so as to properly resolve the regions that are viciously affected, so that the refined O-type mesh remained with the blades as the rotating inner domain rotated relative to the stationary outer domain. The entire domain contains fully structured meshes and the immediate boundary layer around the blades has a first cell height which gives an acceptable range of $y^+ = 0.8 \leq y^+ \leq 5$ and an average of less than one from the flow solutions.
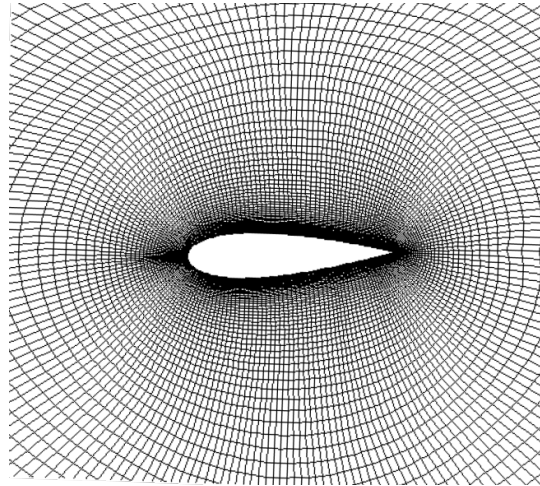
Figure 3. The near blade and O-type mesh around an aerofoil.

The rotating inner domain contains three aerofoils with the nodes concentrated at the leading and trailing edges for a good capture of flow physics (Figure 3 (a, b and c)). The 60-layer O-type mesh around the aerofoils is inflated from the surface of the blade, while the remaining section of the rotating inner domain mesh is generated from the O-type mesh around the aerofoil, both with a growth rate of 1.1. The aerofoil trailing edge is rounded as shown in Figure 4 (b) with an insignificant radius/chord ratio which has no effects on the results. The entire domain is approximately 148,000 cells.
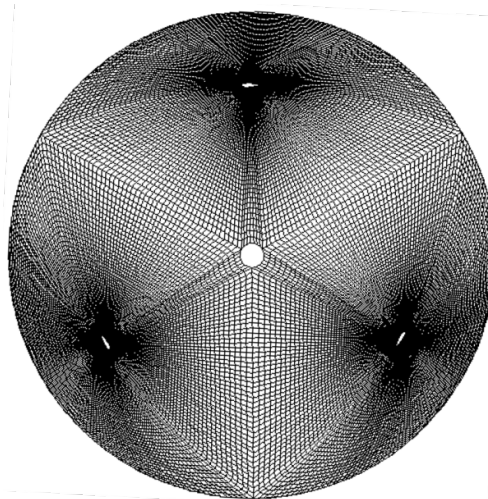
a.
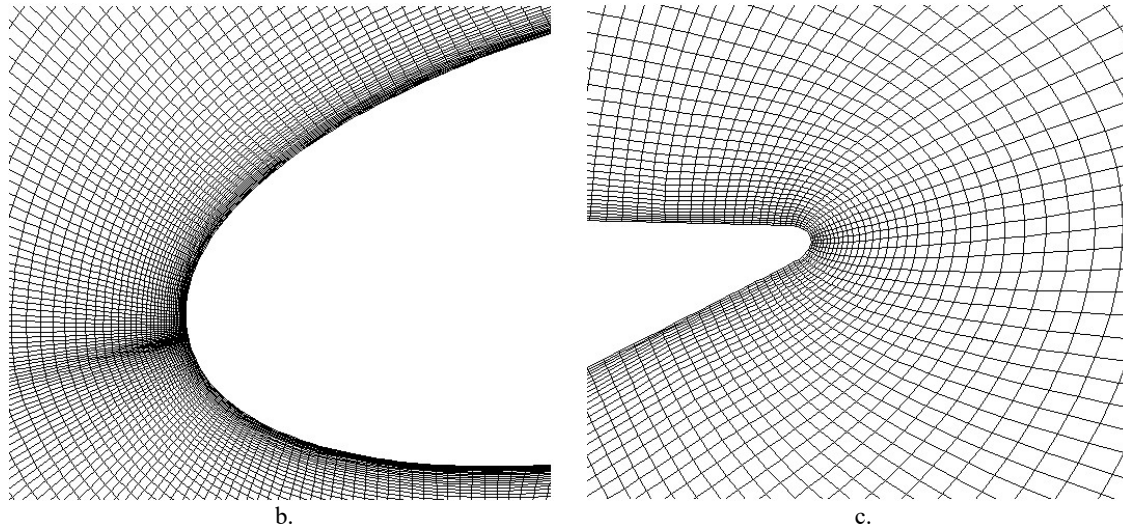
Figure 4. The clustered mesh around a) rotating domain b) leading edge, c) Trailing edge.

The mesh of the outer stationary domain is coarse with 100 nodes only, while the maximum length cell was set to half the length size of blade chord to minimise the computation time (Figure 5). The stationary domain coarse mesh was not considered an issue since the developed wake pattern is outside this study scope. So effects of the presence of a steal matting grid of 2" x 2" and a shuttle mechanism that can generate gusty wind when needed behind the VAWT axis in the wind tunnel set-up, on wake development was not considered.
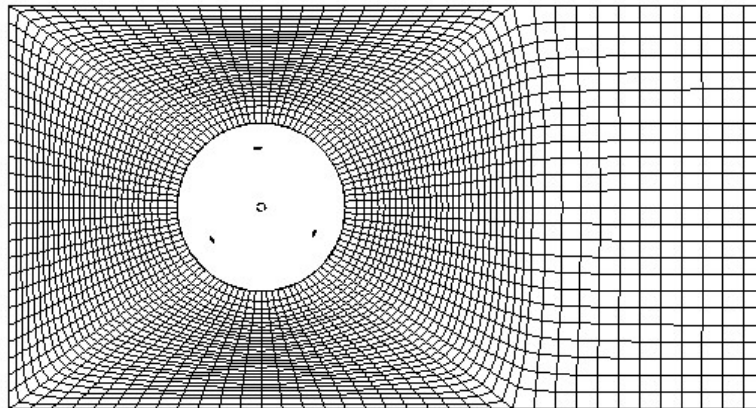
Figure 5. The outer stationary domain mesh

Mesh sensitivity to changes in node number was performed by successively refining the aerofoil surface node density as shown in Figure 6, a method similar to that of Hamada, Smith, Howell, Qin (2008) and Danao, Qin, Howell (2012) was adopted. It was observed that a fine mesh of 400 nodes provided good results at reasonable computational time when compared to a finer 800 node density that consumed approximately three times the computational time at 400 node density. Thus mesh independent was attained at 400 node density level, and is far less than the equally spaced node density required by Amet, Maître, Pellone, and Achard, (2009) and Simão Ferreira, Van Kuik, Van Brussel, (2007).
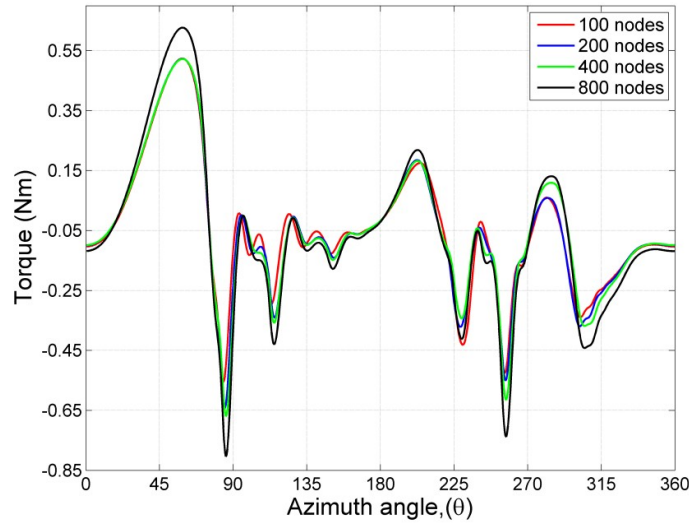
Figure 6: The effects of varying node densities on blade torque at λ = 2.5, and C = 0.04m

Numerical techniques

The numerical investigation has been conducted with the commercial CFD package, Ansys Fluent. The Fluent code solves the fluids governing equations through a finite volume method. The flow is incompressible so a fully unsteady pressure-based coupled solver was selected and all the spatial discretization terms were set to second order Consul, Willden, Ferrer, McCulloch, (2009). The

solution control was set to a courant number of 200 that was high enough to save computational time while allowing reliable convergence. The turbulence intensity was set to $Tu = 8\%$ at the inlet, with a turbulence viscosity ratio of $\mu t/\mu = 14$ that enabled the decay of the turbulence intensity to $Tu = 1\%$ at the immediate region of the blade (Figure 7).
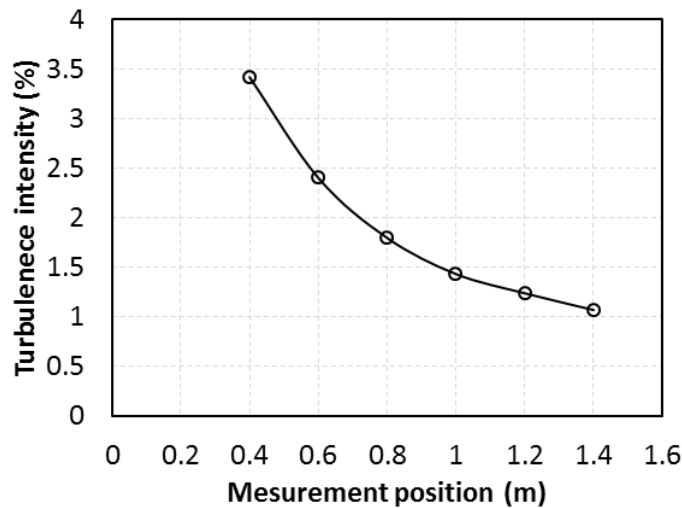
Figure 6: Turbulence intensity decay in the wind tunnel
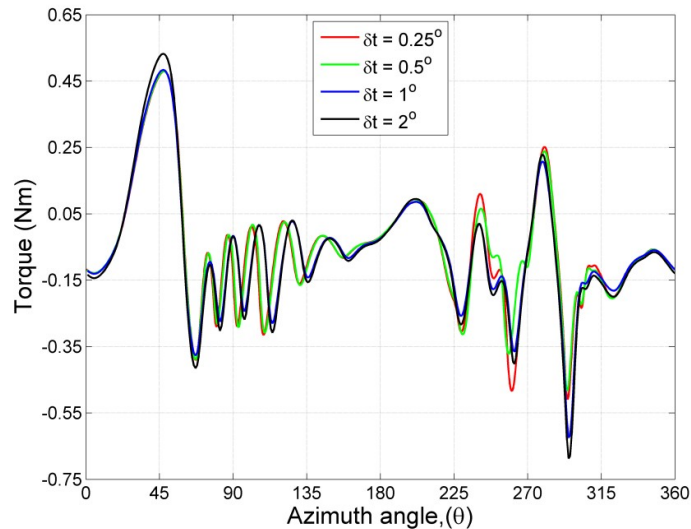
Figure 8. Time step size at various azimuth rotations (δt) at λ = 2.5,

The time step size investigation was varied between δt = 0.25 and δt = 2° at an interval of δt = 0.25°. Based on the required computational time, δt = 0.5° was adjudged most suitable, using time step convergence criteria that was set to residual drop below 1x 10⁻⁴. Figure 8 presents the results of the time step size investigation. δt = 0.5° VAWT's rotation, after time step size and convergence

criteria sensitivity analysis was satisfied was adopted for all the CFD modelling presented in this paper. The simulations were allowed to run for ten full rotations within which partial periodic convergence was observed after four rotations until the seventh rotation where full convergence is seen (Figure 9).
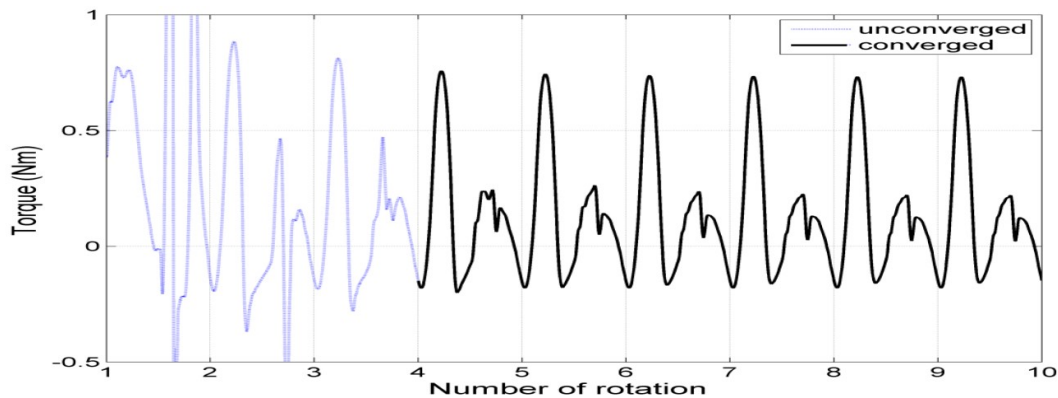
Figure 9. Node densities variation effects on the blade torque generated at λ = 2.5, C = 0.04m

Experimental method
VAWT models

A straight three-bladed VAWT rotor was adapted for the experiments. The VAWT rig has a shaft with 0.027m diameter. The shaft runs from top to bottom of the wind tunnel test section. The shaft is placed 1.8m from the direction of the incoming wind and then 1.2m downwind of test section of the wind tunnel. There are two hubs attached rigidly to the rotor shaft, with provisions for the support arms that connects the blades to the centre shaft. The attached blades to the support arms are 0.35m away from the central shaft. The blades are made of aluminium with the blades

having a NACA0022 profile, while the support arms are NACA0026. The blades are 0.04m chord with solidity = 0.34, and of 0.6m span resulting in aspect ratio of 20 and. The blades are fastened to the shaft via the two support arms at ¼ and ¾ blade length.
Performance measurement technique

The laboratory tests were conducted at the Sheffield University low speed; open-circuit suction wind tunnel. An axial fan installed at the rear of the tunnel drives the flow to a maximum limit of around 25m/s. The working section is 1.2 x 1.2 m² and 3m long and of turbulence intensity Tu = 1% near the rig and a velocity profile of ≤ 0.01%

error which cascaded to ± 1% CP error at λ = 4, at 7m/s wind speed.

The VAWT blade performance was measured using the 'spin down' method, a VAWT performance measuring technique developed by Edwards, Danao, and Howell (2012).The method involves the spinning down of the rotor from a high rotational speed, while the angular velocity monitoring is simultaneous through an optical encoder while the instantaneous acceleration ξ is calculated by Equation (1).

$$\xi = \frac{\omega_2 - \omega_1}{t_2 - t_1}$$

(1)

The rotor rig is spun twice for every test speed to ascertain the aerodynamic forces and VAWT performance. The first and initial spinning down of the rig was to ascertain the resistive torque attained by the rig. The resistive torque T_{res} is determined by spinning the rotor down without the blades attached to measure the system resistance caused by the mechanical friction, bearings and the support arm's induced drag. The blades were not attached to the rig therefore does not require the applying the brakes during the test of all the wind speeds due to negative torque being generated. The T_{res} is computed after the test by using Equation (2).

$$T_{res} = I_{rig}\xi$$

(2)

With the blades attached, a second spinning down test is carried out the total performance of the VAWT in relation to the blade torque. The brake was applied at 7m/s and 8m/s of the three wind velocities tested. The brake application was necessary to prevent the VAWT from cutting-in, a situation where positive torque is generated, so the turbine no longer spins down freely. The blade torque T_B is computed by using Equation (3), the applied torque, $T_{app} = 0$ for cases in which brake power was not applied. Other information of the development and validation of the spin down method are found in Danao (2012).

$$T_B = I_{rig}\xi - T_{res} - T_{app}$$

(3)

$$CP = \frac{P_B}{P_w}$$

(4a)

$$P_B = T_B\omega N$$

(4b)

$$P_w = 0.5\rho A V_w^3$$

(4c)

The power performance of the Rig from the torque attained by the blade was computed by Equation (4a -4c) after determining the T_B from the spin-down tests.

Flow field measurement technique

Particle image velocimentry (PIV) is a method wherein the instantaneous flow velocity within

field of view (FOV) is visualised and measured through the introduction of buoyant particles of very small diameter to the fluid stream. The particles in the wind stream, illuminated by a laser sheet, are assumed to faithfully follow the fluid velocity, and their motion captured by using a sensitive charged coupled device (CCD) camera. Flow velocity was measured as a ratio of displacement of the particles and time interval between two closely captured images. The time interval between the two images is such that the displacement of the particles is a quarter of the interrogation window dimension.

The set-up of the PIV equipment for the campaign, detailed in Eboibi (2013), is such that the camera and the laser are perpendicular in alignment. Reflection was reduced with the (CCD) camera aligned in the perpendicular plane of the image. A marked disc with 36 azimuth angles representing the 360° of a full rotation at 10° intervals is fixed to the camera rig and the VAWT encoder so the camera and the VAWT can be rotated to various angles within reasonable accuracy.

The laser position was moved around to retain the initial set alignment at the desired azimuth angle being tested. The CCD camera was positioned radially so that the blade was centred in the camera view and also the chord line parallel to one edge of the FOV. The seeding generator generates the small buoyant particles upstream, in front of the tunnel. The University of Sheffield open suction low speed wind tunnel with 1.2 x 1.2 m² and 3m long working section was the test cell. The transparent sides of the tunnel were covered with non-transparent blinds for safety and health of personnel in the laboratory, while the experiment is being conducted.

The accuracy with which the tracer particles follow fluid stream was determined by estimating the seeded particles settling velocity in relation to the free stream fluid motion through Equation (5). The tracer particle settling velocity was estimated to be 0.0001m/s which are very negligible when compared to the 6m/s wind speeds at which the PIV test and investigation were carried out, signifying that the particles would follow the fluid motion faithfully without moving from the fluid streamlines even during periods of rapid randomness in flow direction as a result of separation of flow.

$$v_s = \frac{2gR_p^2\left(\rho_p - \rho_f\right)}{9\mu_f}$$

(5)

The blade surface was treated to achieve a tolerable level of reflection even after proper placement of laser sheet source and the CCD camera, to prevent damage of the camera, and having an insignificant impact on the results accuracy, since proper setting and alignment of the

camera and the laser can only reduce the reflection level from the blade surfaces. After the blade treatment, various verification of test settings that includes laser sheet thickness, height of laser sheet with relation to blade position, seeding concentration, laser power, time between pulses and number of ensembles were carried out to select appropriate test parameters of the main experiments.
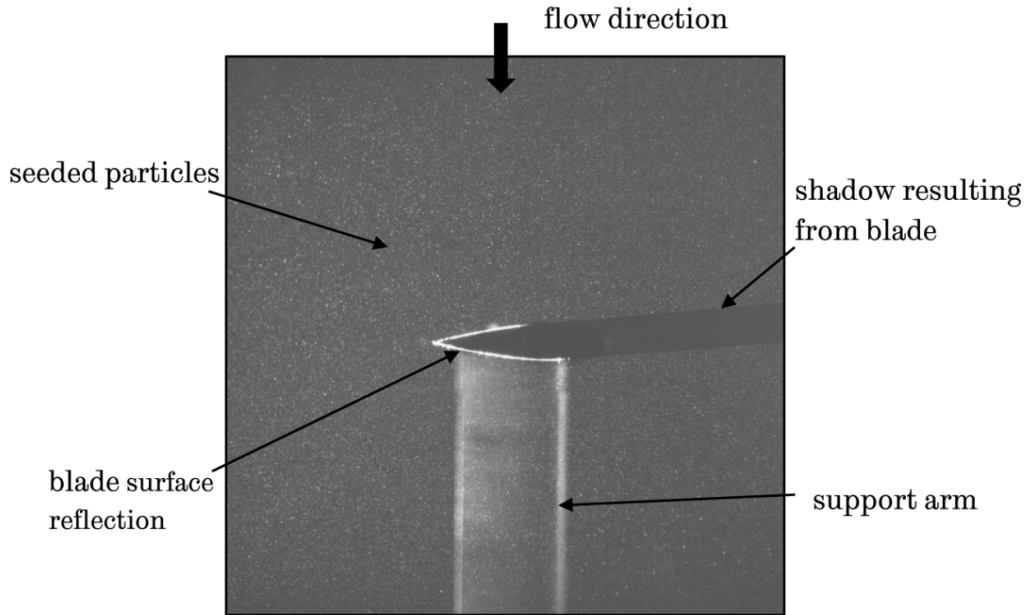
Figure 10. Raw PIV data sample at a 90° and 6m/s in the FOV

The analysed acquired data (Figure 10), following an analysis sequence detailed in Eboibi et al, (2015) yielded a 2D vorticity plots (Figure 11). Flow field vorticity around a blade was adopted over velocity streamlines because it can best describe the clockwise and anti-clockwise movements of the seeded particles in the stream of flow around the blade environment over the velocity streamlines by relating particle circulation in the interrogation windows to the FOV area (Equation 6).
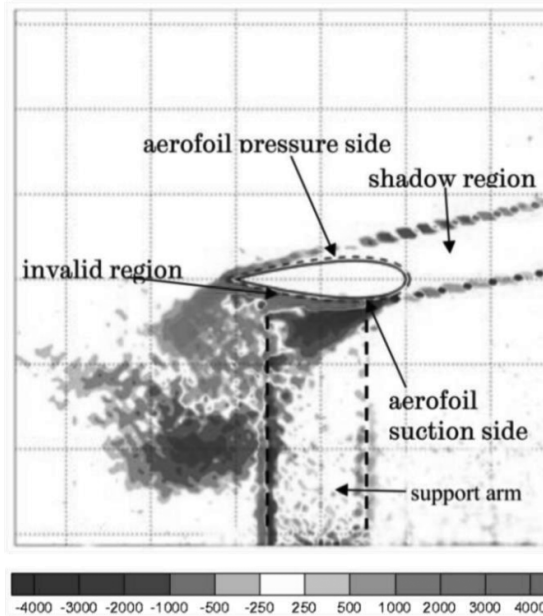
Figure 11: Sample of vorticity plot of the vectors statistics at 6m/s, θ=90°, C =0.04m at λ = 2.5.

$$\text{vorticity}(\zeta) = \frac{\text{circulation}(\Gamma)}{\text{area}} = \frac{\partial v}{\partial x} - \frac{\partial u}{\partial y} \qquad (6)$$

Results

Force validation

Evaluation and comparing CFD solutions to standard results (experimental results in most cases) authenticates the validity of CFD models, influences the turbulence models choice and selection, level of solution accuracy and the computational time. Danao, Qin, Howell (2012) validated their models with a pitching aerofoil experiment data at an average Reynolds number of 1.35 x10⁵. Validation of CFD models against pitching aerofoil alone is not sufficient to either confirm validity of the numerical and CFD model or make an appropriate choice of a turbulence model.
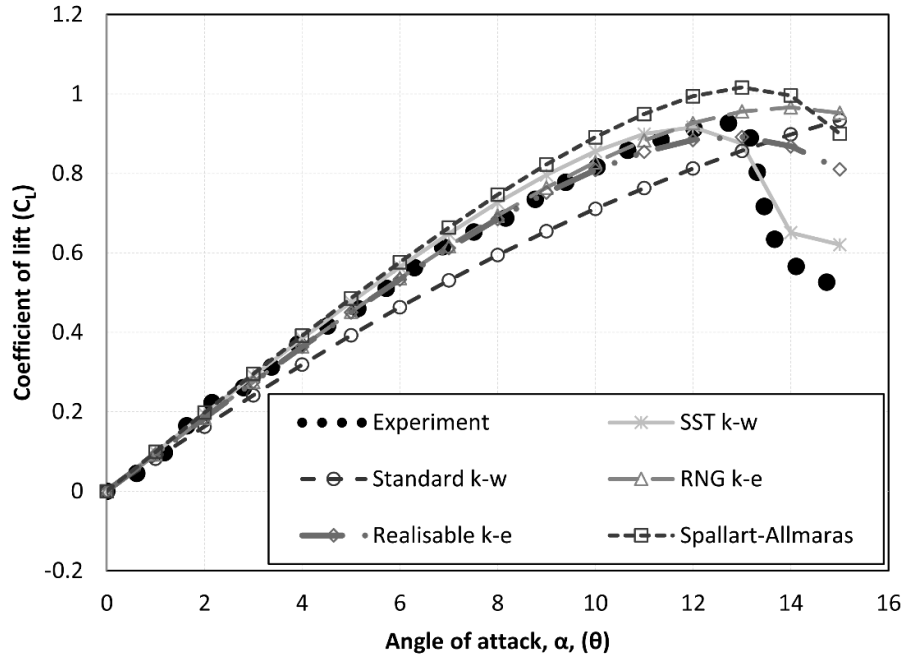
Figure 12. Coefficient of lift versus angle of attack for five turbulence models.

To properly investigate the suitability of CFD model, a thorough validation campaign was initiated with a static aerofoil study that was aimed at reducing the list of available turbulence models. Five fully turbulent models were tested against the experimental data of Sheldhal and Klimas (1981) at Reynolds number of 1.35×10^5. The turbulence models tested were the one equation S-A, Standard $k - \omega$, SST $k - \omega$, Realisable $k - \varepsilon$ and RNG $k - \varepsilon$. The static aerofoil study was achieved by simulating a 2D NACA0012 profile of 0.15m chord at 13.67m/s in similar conditions that the experiment was conducted. An appropriate first cell height that yields a $y^+ \leq 45$ for the models that required wall treatment and a $y^+ \leq 1$ for models without wall treatment was implemented. Figure 12 shows the static aerofoil study results with the SST $k - \omega$ showing best prediction of the obtained experimental data over the other turbulence models, especially at the high angle of attacks. The inherent nature of the SST $k - \omega$ model being able to predict flows in the near blade and far field regions based on Menter (1993) investigation, may have influenced its better predictability of the laboratory and experimental data.
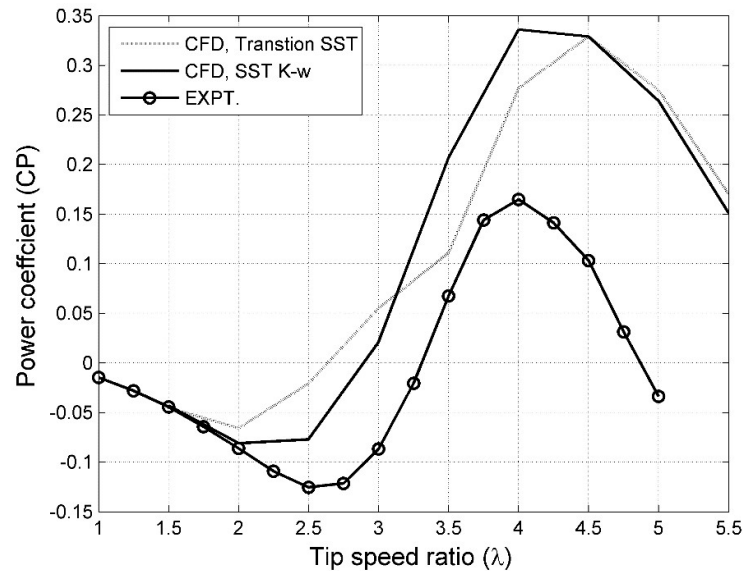
Figure 13. Comparison of CP curves at 6m/s, C = 0.04m.

After the static aerofoil investigation, a wind tunnel small scaled three bladed VAWT power coefficient and the flow fields were measured experimentally by a performance measurement technique and Particle Image Velocimentery (PIV) measurement method presented earlier in the previous sections. The developed CFD model was simulated at the similar test conditions of 6.0m/s that the experiments were conducted. Also, a 2D created CFD model of a visual wind tunnel scaled VAWT was simulated using the SST $k-\omega$ turbulence model that best predicted static aerofoil experimental data. Also, a Transitional SST turbulence model was introduced to simulate the developed CFD model because Transition SST turbulence model has the attributes of accurately predicting flows within transition region. The laboratory experimental data obtained at low Reynolds numbers (ranging from 16,800 to 84,000), explains why the Transition SST turbulence model is included for the verification and validation campaign.

Figure 13 showed Transition SST and fully turbulent SST $k-\omega$ turbulence models over predicted the experimental CP at all the tip speed ratios except at $\lambda = 1.5$ where convergence of the three curve is seen. At the low λ region, negative performance is seen in the curves up to $\lambda = 2.7$ where the Transition SST model deviated and started attaining positive performance which peaked at CP = 0.325 at $\lambda = 4.5$. The fully turbulent SST $k-\omega$ is seen with a deeper negative trough than the Transitional SST. The fully turbulent SST $k-\omega$ maintained a steady rise in power coefficient until a maximum CP = 0.34 at $\lambda = 4$ is attained.

Notable in the peak performance region of $\lambda = 3.5$ to $\lambda = 4.5$ is the Transitional SST seen closer to the experiment than the fully turbulent SST $k-\omega$ signifying better prediction in this region by the transitional SST than the fully turbulent SST $k-\omega$ model. The peak performance region is usually of importance to the designer because of its effects on the economic returns associated with energy yield of wind machines harvesters.

At $\lambda = 4.5$ and beyond the difference in the performance between the two turbulence models is negligible. The curves are seen to converge at $\lambda = 4.5$ and with little separation as they move further with increase in tip speed ratios. From the Figure 11 the experiment is best predicted by Transitional SST at the peak power region while the fully turbulent SST $k-\omega$ best predicted the power coefficient of the lower λ especially at the negative performance region.

Over prediction of the experimental curve seen in the Figure 13 by the two CFD models is caused by the two dimensional design of the models being compared to 3D experimental data. The over predictions of the experimental results by 2D CFD models have previously been observed in literature. Howell, Qin, Edwards, Durrani (2010) adopted Realisable $k-\varepsilon$ turbulence model to 2D and 3D CFD models and results obtained were then compared with the experimental results on a similar VAWT scale. The 2D CFD model over predicted their experimental data at all tip speed ratios tested whereas under prediction of experimental power curves by the three dimension CFD model at higher tip speed ratios were observed.

In a similar study by Raciti-Castelli et al, (2011) in which the Realisable $k-\varepsilon$ turbulence model was used, and Edwards, et al., (2012) that adopted

the fully turbulent SST $k-\omega$ model, their experimental power curve was over predicted by 2D CFD models. Danao et al., (2012) study although showed good prediction at some tip speed ratios due to the introduction of Transition SST model, their two dimensional CFD model equally over predicted their experimental data in most of the compared tip speed ratios. Common in all these studies is the higher over prediction of experimental data at higher tip speed ratios by 2D CFD models. 2D CFD models over prediction of experimental data observed in all these studies can been adduced to the infinite blade span effects of 2D CFD models and the finite blade span and support arm effects of 3D experimental VAWT. Tip vortices shed by the 3D models are the main reasons for the difference in performances observed between the 2D and 3D models, because the shed tip vortices induced drag led to the decrease of overall performance efficiency of 3D models. All these studies compared well with the power coefficient validation campaign in this investigation to determine the suitability of two dimensional CFD models of VAWT.

Flow physics validation

The comparison of the flow physics of the two CFD turbulence models against the PIV measured data was the second part of the verification and validation campaign. This is aimed at justifying the selection of an appropriate CFD turbulence model that best compared well with the experimental results since flow physics can influence and determine the performance efficiency of VAWT (Eboibi et al, 2016), so power coefficient validation

alone is not sufficient to make an appropriate choice of CFD turbulence model.

Figure 14 shows plots of vortices around a blade for Transition SST, fully turbulent SST $k-\omega$ and the PIV experiments. Separation bubble from the trailing edge is seen at $\theta = 70^o$ in the PIV indicating the blade stalling onset. Onset of stall is equally seen in the Transition SST and the fully turbulent SST $k-\omega$. While the separation bubble formation is seen more advanced for the Transition SST, it is delayed in the SST $k-\omega$.

At $\theta = 80^o$, the flow structures of the PIV is better captured by the Transition SST. LEV is developed fully and gradually being pushed from the surface of the blade by the formation of the TEV. The flow around the fully turbulent SST $k-\omega$ has separation bubble that is seen developed to LEV but with delayed formation of TEV which implies delayed stalled. At $\theta = 90^o$, it is seen and can be deduced in the PIV data that the first LEV developed detaches from the surface of the blade, followed by initial development of a second separation bubble, while the roll up of the TEV has advanced. This is well captured by the Transition SST that showed a robust development of the TEV being more advanced. About 10° phase difference is observed between the PIV and the fully turbulent SST $k-\omega$ with later lagging behind. At $\theta = 130^o$, a resemblance is seen in the two CFD turbulence models showing detachment and the shedding of the pairs of noticeable vortices which is equally seen in the PIV, implying that the PIV data are well captured by the two turbulence models at this azimuth position.
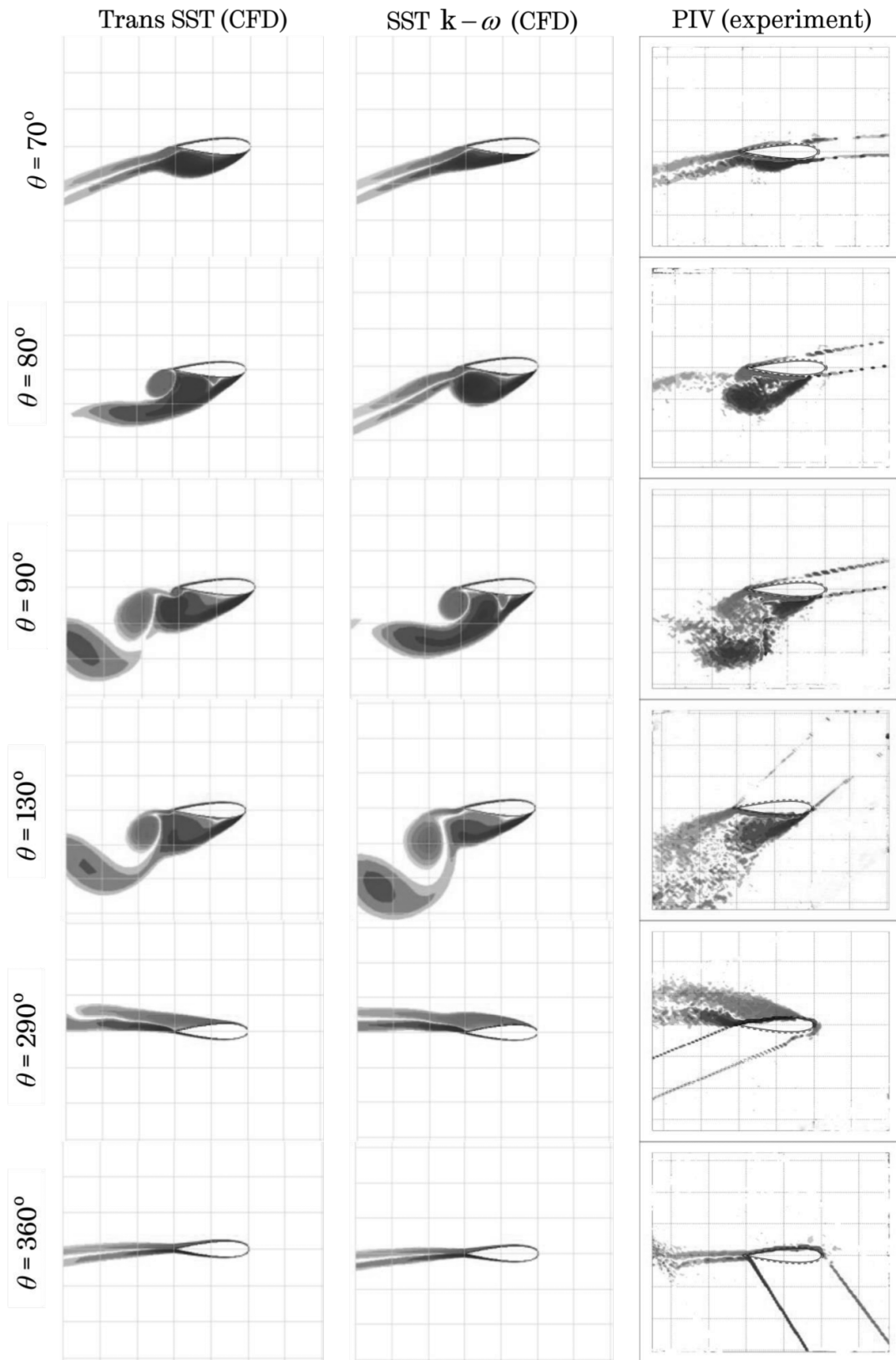
Figure 14. Vorticity plots of flow fields around a blade at 6m/s for various azimuth angles, λ = 2.5, C = 0.04, σ = 0.34.

At θ = 290º, shedding of robust vortices that is followed by an onset of reattachment the flow to the surface of the blade is seen in the PIV while the

Transition SST and SST $k-\omega$ have their boundary layers attached to surfaces the blade. At θ = 300° all flow fields, including that of the PIV are attached to the surface of surface. Overall the Transition SST is a better choice judging from the better capture of the PIV than the fully turbulent SST $k-\omega$ at some of the azimuth positions. The best performance can be adduced to the ability of the Transitional model in capturing the flow in the transitional region especially from start of the rotation until θ = 130° when the flow became turbulent.

Conclusion

The suitability of using a numerical CFD model for research purposes has been presented. A CFD VAWT was create and simulated. A three bladed VAWT was developed and tested in a wind tunnel. The power and flow field parameters were obtained and compared with those of those of the numerical simulation.

The turbulence modelling exercise in which five models were tested against experimental data of a NACA012 static aerofoil has shown that the SST $k-\omega$ turbulence was the most appropriate model of the five candidates tested. A further comparison of the SST $k-\omega$ and Transition SST with experimental power coefficient data of the VAWT showed a better prediction at the lower λ by the SST $k-\omega$, while the Transition SST prediction at the higher λ is better for the C = 0.04 VAWT.

The flow physics validation especially at the λ = 2.5 showed the Transitional SST as the better turbulence model since it best captured the PIV features in most azimuth positions compared in the incoming wind section of the free stream flow than the fully turbulent SST $k-\omega$. Judging from the force and flow physics validations, the Transition SST turbulence model is the most appropriate model for the CFD modelling in the Reynolds numbers rang the investigation was conducted. Therefore the numerical models are suitable for research purposes if properly verified and validated with genuine experimental data.

References

Amet E., Maître T., Pellone C., and Achard J. L., (2009). 2D numerical simulations of blade-vortex interaction in a Darrieus Turbine, *Journal of Fluids Engineering*, 131(11), pp. 111103-15.

Consul C.A., Willden R.H.J., Ferrer E., McCulloch M. D., (2009). Influence of solidity on the performance of a cross-flow Turbine, *Proceedings of the 8th European Wave and Tidal Energy Conference, Uppsala, Sweden.*

Danao L. A. M., (2012). The influence of unsteady wind on the performance and aerodynamics of vertical axis wind turbines, Ph.D. Thesis, *University of Sheffield, Sheffield, UK.*

Danao L.A., Qin, N., Howell, R., (2012). A numerical study of blade thickness and camber effects on vertical axis wind turbines, *Proceedings of the institution of Mechanical Engineers, Part A: Journal of Power and Energy*; pp 15-22.

Eboibi O., (2013). The influence of blade chord on the aerodynamics and performance of vertical axis wind turbines, PhD Thesis, *The University of Sheffield, Sheffield, United Kingdom.*

Eboibi O., Edwards J., Howell R., Danao L.A. (2015). Visualising Dynamic Stall around a Vertical Axis Wind Turbine Blade Through Particle Image Velocimetry. In: Yang, GC., Ao, SI., Gelman, L. (eds) Transactions on Engineering Technologies. Springer, Dordrecht. https://doi.org/10.1007/978-94-017-9804-4_16

Eboibi O., Danao L.A. and Howell R.J., (2016). Experimental Investigation of the Influence of Solidity on the Performance and Flow Field Aerodynamics of Vertical Axis Wind Turbine at Low Reynolds Numbers. Renewable Energy. Vol. 99: pp. 474 – 483.

Eboibi B.E, Eboibi O.Okubio E., Iyasele C. (2017). Evaluation of wind energy potential in the south – south geopolitical zone of Nigeria. Journal of Applied Science and Environmental management 27 (7) 1301 – 1306.

Eboibi B. E, Eboibi O., Okputu J.Okpohwo K.A. (2018). Production of and analysis of biodiesel Jatropha curcas seed. Journal of Applied Sciences and Environmental Management. 22 (1) 26 - 33

Edwards J.M., Danao L.A., and Howell R. L., (2012). Novel Experimental Power Curve Determination and Computational Methods for the Performance Analysis of Vertical Axis Wind Turbines, *Journal of Solar Engineering,* 134(3), pp.11-18

Hamada K., Smith T., Howell R., Qin N., (2008). Unsteady flow simulations and dynamic stall around vertical axis wind turbine blades. *27th ASME Wind Engineering Symposium, 2008 AIAA-2008-1319.*

Howell R., Qin N., Edwards J., Durrani N., (2010). Wind tunnel and numerical study of a small vertical axis wind turbine. *Renewable Energy.* **35**(2): pp. 412-422.

Jian C, Liu C, Hongtao X, Hongxing Y, Changwen Y, Di L. (2016). Performance improvement of a vertical axis wind turbine by comprehensive assessment of an airfoil family. Energy, 114, 318 - 331

Menter F. R., (1993). Zonal two equation k-w turbulence models for aerodynamic flows, *Aerospace Sciences Meeting and Exhibition, January 11-14, Reno, Nevada.*

Raciti Castelli, M., Englaro A., Benini, E., (2011). The Darrieus wind turbine: proposal for a new performance prediction model based on CFD. *Energy,* **36** (8) pp. 4919-4934.

Raciti Castelli, M., Ardizzon, G., Battisti, L., Benini, E., and Pavesi, G., (2010). Modelling strategy and numerical validation for a darrieus vertical axis micro-wind turbine, *ASME Conference Proceedings, pp. 409- 418*.

Simão Ferreira C. J., Van Kuik G., Van Brussel G. J. W., (2007). 2D CFD simulation of dynamic stall on a vertical axis wind turbine: verification and validation with PIV measurements, *in 45th AIAA Aerospace Sciences Meeting and Exhibition, Reno, Nevada*.

Shedahl, R.E., Klimas, P.C., (1981). Aerodynamic characteristics of seven symmetrical airfoil sections through 180-degree angle of attack for use in aerodynamic analysis of vertical axis wind turbines, Sandia national laboratories: Albuquerque, New Mexico.

Qing'an Li, Takao M., Yasunari K., Junsuke M. Kazuma F., (2016). Measurement of flow field around straight-bladed vertical axis wind turbine. Journal of Wind Engineering and industrial Aerodynamics, 151, 70-78.

Sungjun J, Heungsoap, Juhee L. (2015). Aerodynamic characteristics of two-bladed H-Darrieus at various solidities and rotating speeds. Energy, 90, 439 – 451.